Soft Matter

PAPER

View Article Online
View Journal | View Issue

Cite this: *Soft Matter*, 2022, **18**, 4265

Active depletion torque between two passive rods

Longfei Li,[ab] Peng Liu,[bcd] Ke Chen,[bce] Ning Zheng *[a] and Mingcheng Yang *[bce]

Received 13th April 2022,
Accepted 8th May 2022

DOI: 10.1039/d2sm00469k

rsc.li/soft-matter-journal

The active depletion torque experienced by two anisotropic objects in an active bath is a conceptional generalization of the equilibrium entropic torque. Using Brownian dynamics simulations, we compute the active depletion torque suffered by two passive rods immersed in an ensemble of active Brownian particles. Our results demonstrate that the active depletion torque is qualitatively different from its passive counterpart. Interestingly, we find that the active depletion torque can be greatly affected by the external constraint applied on the rotational degree of freedom of the rods, and even the direction may be changed with the orientational constraint, which is in contrast to the equilibrium depletion torque. The main reason for the remarkable features of the active depletion torque is that the active particles can significantly accumulate in the vicinity of the rods due to persistent self-propulsion, which is sensitively dependent on the constraint strength and the rod configurations. Our findings could be relevant for understanding the self-assembly and dynamics of anisotropic macromolecules in living environments.

I Introduction

Active matter, ranging from cell cytoskeleton filaments[1] and bacteria colonies[2–5] to artificial microswimmers[6–12] and shaken non-symmetric granular particles,[13,14] are composed of active units that individually convert the stored or environmental energy into autonomous motion.[15–18] Due to being inherently out-of-equilibrium, active matter can exhibit striking phenomena, such as motility-induced phase separation,[19–23] novel self-organization[24–27] and spontaneous collective motion,[5,28–31] which is absent in passive systems.

Because of the irreversibility of persistent self-propulsion, which is fundamentally different from irregular thermal motions, active-matter systems often have abnormal mechanical and thermodynamical properties. For example, pressure in active matter is generally not a state function, except for some specific models, *i.e.*, spherical active Brownian particles without orientational coupling with the boundary walls.[32] The active noise experienced by a passive intruder in a fluid of self-propelled particles is not the intrinsic attribute of the active bath, but depends on the external potentials applied to the intruder.[33] Moreover, the active bath is able to exert a net torque on chiral passive intruders and thus drive their unidirectional rotation,[34–37] which only suffer from stochastic rotation in a thermal bath.

In addition to producing direct forces or torques, the active bath can mediate effective interactions between immersed passive objects. A particularly important example is the active depletion force that is a conceptual extension of the equilibrium depletion force. Interestingly, the active depletion force substantially changes with the external constraint suffered by the passive objects,[38] in contrast to its equilibrium counterpart that is of entropic origin and independent of the dynamics of suspended objects.[39] In other words, the active effective interaction between the free passive objects is not equivalent to that between the fixed objects, although this equivalence has been widely employed to determine the equilibrium entropic force. Given that activity-mediated self-assembly has recently stirred up considerable interest,[40–44] and as biological self-assemblies (such as the biological "key–lock" mechanism forming a bond between non-spherical macromolecules[45]) usually occur in living environments,[46,47] it is thus necessary and important to understand deeply the characteristics of the active effective interactions.

Nevertheless, relative to the active depletion force that has been extensively studied,[38,48–51] investigation of the active depletion torque between non-spherical passive objects is rare.[52,53] In equilibrium, the depletion torque arises from the entropic effect[54–59] and plays a vital role for the self-assembly of anisotropic objects.[60–63] The equilibrium depletion torque can

[a] School of Physics, Beijing Institute of Technology, Beijing 100081, China. E-mail: ningzheng@bit.edu.cn
[b] Beijing National Laboratory for Condensed Matter Physics and Laboratory of Soft Matter Physics, Institute of Physics, Chinese Academy of Sciences, Beijing 100190, China. E-mail: mcyang@iphy.ac.cn
[c] School of Physical Sciences, University of Chinese Academy of Sciences, Beijing 100049, China
[d] Wenzhou Institute, University of Chinese Academy of Sciences, Wenzhou, Zhejiang 325001, China
[e] Songshan Lake Materials Laboratory, Dongguan, Guangdong 523808, China

be either characterized by the orientational distribution function of two freely rotating non-spherical objects, or equivalently determined by measuring the torques on two fixed objects exerted by the depletants. However, in the context of an active bath that is far from equilibrium, it is unfeasible to obtain the active depletion torque from the orientational distribution function. On the other hand, the active depletion torque perhaps is constraint-dependent, similar to the case of the active depletion force, which may disable the measurement of the active depletion torque on free objects with the strategy of fixing objects. The observations thus raise a natural question: how does the external constraint influence the active effective torque?

In this paper, we numerically investigate the active depletion torque experienced by two passive colloidal rods in a two-dimensional fluid of active particles. In particular, we study the effect of the external conditions on the active depletion torque using an angle potential to confine the rod orientation, which roughly mimics external environments that influence the rotational dynamics of the rods, like diverse viscoelastic or crowded media. Compared with the equilibrium case that is independent of the external conditions, the active depletion torque not only has a much larger magnitude but also significantly hinges on the constraint potential. Moreover, both the direction and magnitude of the active depletion torque change sensitively as the rod configurations and orientations vary. The complex behavior of the active depletion torque can be explained based on the joint effects of the entropy-like torque and the motility-induced accumulation of active particles in the concave region formed by the two rods. The constraint dependence of the active depletion torque could open up new possibilities to manipulate non-symmetric objects and direct activity-induced self-assembly.

II Simulation systems

The two-dimensional active bath is composed of 1000 active Brownian particles of diameter σ_a, with a packing fraction ρ = 0.2 to avoid motility-induced clustering. The colloidal rod is simulated as a spherocylinder with a width $\sigma_r = 1.5\sigma_a$ and cylindrical length $l = 4.5\sigma_a$, as sketched in Fig. 1(a). Throughout the simulations, the rod centers are fixed with a distance d between the two rod centers, and the orientation of the rod is described by the included angle between the long axis of the rod and the line connecting the two rod centers, θ_{le} and θ_{re}, which respectively correspond to the left and right rods. According to the system symmetry, we focus on three types of rod configuration [see Fig. 1(b–d)]: symmetric configuration I ($\theta_{le} = 180^\circ - \theta_{re}$), parallel configuration II ($\theta_{le} = \theta_{re}$) and asymmetric configuration III ($\theta_{le} = 90^\circ$). The three configurations are the most representative and cover most of the typical configurations of two rods. Choosing the three configurations thus facilitates a comprehensive exploration of the possible constraint dependence of the active depletion torque, with a relatively low computational cost. For convenience, we also

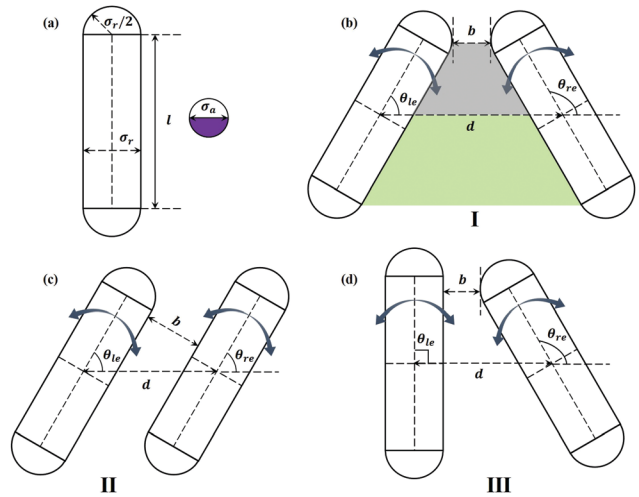

Fig. 1 (a) Sketch of a passive rod and an active Brownian particle moving toward the purple side. Three types of rod configurations used in simulations: (b) symmetric configuration I, (c) parallel configuration II and (d) asymmetric configuration III. Here, θ_{le} and θ_{re} represent the orientations of the left and right rods relative to the line connecting the two rod centers, respectively, and d is the separation between the two rod centers. The thick arrows describe the orientational fluctuations of the rods under the external angle potentials. Note that for configuration I in (b), the gray and light-green regions signify the upper and lower concave areas between the two rods, respectively.

identify the shortest surface separation between the two rods as b. All the inter-particle, particle–rod and rod–rod interactions (U_{pp}, U_{pr}, U_{rr}) are modelled using a Weeks–Chandler–Andersen potential, $U(r) = 4[(\sigma/r)^{12} - (\sigma/r)^6] + 1$ if $r < 2^{1/6}\sigma$ and $U(r) = 0$ otherwise, separately with the interaction diameter $\sigma = \sigma_a$ for U_{pp}, $\sigma = [\sigma_a + \sigma_r]/2$ for U_{pr}, and $\sigma = \sigma_r$ for U_{rr}. In order to investigate the influence of the external constraint environment on the effective torque, the rotational degree of freedom of each rod is independently coupled to an external torsion spring, $\frac{k_\theta}{2}(\theta - \theta_o)^2$, with θ_o being the equilibrium orientation and k_θ the spring stiffness.

The position $\mathbf{r}_i$ and orientation $\mathbf{n}_i = (\cos\phi_i, \sin\phi_i)$ of active particle i are updated *via* overdamped Langevin equations

$$\begin{aligned} \gamma_t \dot{\mathbf{r}}_i &= F_d \mathbf{n}_i - \nabla_{\mathbf{r}_i} U_t + \sqrt{2k_B T \gamma_t}\boldsymbol{\xi}_i, \\ \gamma_r \dot{\phi}_i &= \sqrt{2k_B T \gamma_r}\zeta_i \end{aligned} \tag{1}$$

with $\gamma_t(\gamma_r = {\sigma_a}^2\gamma_t/3)$ being the translational (rotational) friction coefficient, $k_BT = 1$ being the thermal energy, F_d being the self-propelling force taken as $F_d\sigma_a/k_BT = 20$ in simulations, and $U_t(r)$ being the steric interactions. Here, $\boldsymbol{\xi}$ and ζ are the Gaussian-distributed white noise of the zero mean and the unit variance.

We take the left rod as an example to describe the evolution of the rod orientation in the simulations. Similarly, the rod orientation evolves *via* the overdamped Langevin equation

$$\gamma_w \dot{\theta}_{le} = M - \partial_\theta\left[\frac{k_\theta}{2}(\theta_{le} - \theta_{lo})^2\right] + \sqrt{2k_B T \gamma_w}\zeta, \tag{2}$$

where ∂_θ refers to the derivative with respect to the rotational degree of freedom, and $\gamma_w = \gamma_0(\ln p - 0.662 + 0.917/p - 0.050/p^2)^{-1}$

refers to the rotational friction coefficient of the rod,[64] with $p = l/\sigma_r + 1$ and $\gamma_0 = \gamma_t (l + \sigma_r)^3/9\sigma_a$. Here, M contains the active depletion torque M_e (only a conceptual extension of the equilibrium depletion torque) arising from the active particle–rod collisions and the torque contributed by the rod–rod interactions. The last term of eqn (2) is the stochastic torque on the rod. In the simulations, the rod orientation fluctuates around its equilibrium position determined by the external angle potential, and the active depletion torque is measured and averaged when the deviation of the rod orientation from its equilibrium angle is lower than 0.5°, *i.e.*, $|\theta_{le} - \theta_{lo}| < 0.5°$ and $|\theta_{re} - \theta_{ro}| < 0.5°$. By tuning the spring stiffness, we can achieve different strategies to measure the depletion interactions. For instance, $k_\theta = \infty$ and $k_\theta = 0$, respectively, correspond to the frozen and free schemes, both of which are equivalent in the equilibrium state.

III Results and discussions

3.1 Active depletion torque for configuration I

We first compute the active depletion torque M_e on the two rods for configuration I. We choose a moderate center-to-center distance $d = 4.0\sigma_a$. Due to the symmetry, the orientation angle θ_{le} of the left rod is varied from 59.0° to 90.0° ($\theta_{re} = 180° - \theta_{le}$), where the minimum θ_{le} is determined when the two rods touch. Fig. 2(a) shows M_e as a function of θ_{le} for various reduced constraint strength values $k = k_\theta/k_BT$ ranging from 0 (freely rotating rods) to infinity (fixed rods). For comparison, Fig. 2(a) also plots the corresponding equilibrium depletion torque (namely $F_d = 0$), which is computed only for infinite k_θ because of its independence of the external constraint. As the two rods in configuration I experience opposite torques, we only consider the torque on the left rod.

Remarkably, M_e with infinite k_θ is generally orders of magnitude larger than the passive value, and even the direction of M_e is opposite to its passive counterpart for most orientations. More interestingly, the whole profile of M_e rises with increasing constraint strength k_θ (namely M_e becomes more positive) [Fig. 2(a)], accompanied by a reversal of the torque direction at small orientational angles. This constraint dependence is similar to the case of the active depletion force[38] but is fundamentally distinct from the passive depletion torque that is independent of the constraint. In order to understand the unusual behavior, we qualitatively analyze the origin of the active depletion torque in the following.

Compared with the equilibrium depletion torque (also called the entropic torque owing to its entropic origin), there basically exist two different contributions to the active depletion torque. On the one hand, the rods experience strong collisions with the active particles due to their self-propulsion. Using the idea of the effective temperature, the strong collisions can be roughly approximated as those from the passive particles with an enhanced effective temperature T_e related to the motility of active particles through $k_BT_e = k_BT + F_d^2\tau_r/2\gamma_t$[32,65,66] (with $\tau_r = \gamma_r/k_BT$ the reorientation time of the active particle). Thus, the

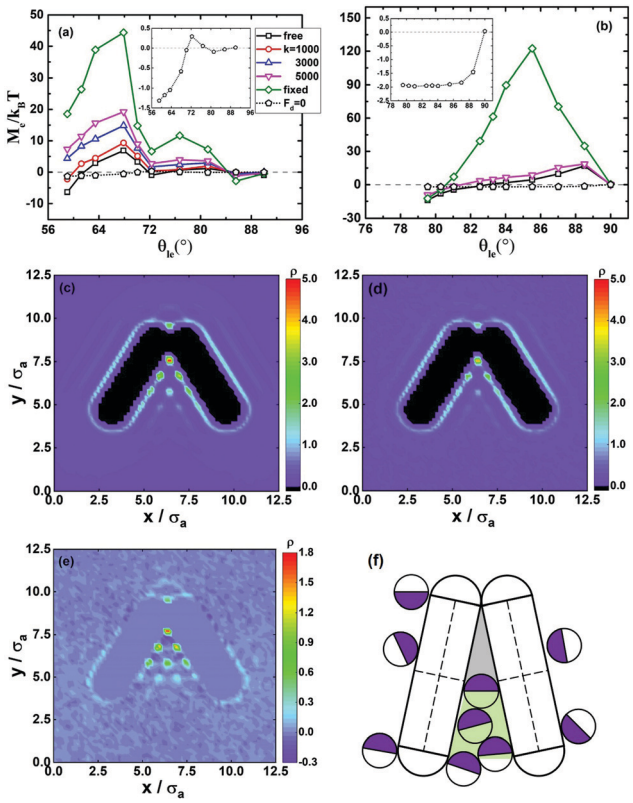

Fig. 2 Configuration I. The reduced active depletion torque M_e/k_BT as a function of the orientation θ_{le} of the left rod with various normalized spring stiffness values $k = k_\theta/k_BT$ at (a) $d = 4.0\sigma_a$ and (b) $d = 2.5\sigma_a$. Insets: The passive depletion torque is shown for clarity. Here, the positive torque is counterclockwise. The typical density maps of the active particles for (c) fixed and (d) free rods, with the separation $d = 4.0\sigma_a$ and orientation $\theta_{le} = 59.0°$, and (e) the corresponding density difference map between (c) and (d). (f) Mechanism of the 'self-locking' effect.

effective torque on the rods arising from the strong collisions can be approximately regarded as that in an equilibrium system with the effective temperature T_e, which is referred to as the entropy-like torque M_e^e. The entropy-like torques are usually inclined to rotate the rods to bring them into contact (clockwise or negative M_e^e), similar to (but much larger than) the equilibrium entropic torque. On the other hand, the concave region formed by the two rods can trap the active particles due to their persistent motions, leading to an accumulation of active particles, which strengthens with the Peclet number of the active particle.[51,67] This accumulation effect can also contribute to an effective torque on the rods, called the accumulation torque M_e^a. So, the active depletion torque M_e is approximately a superposition of the above two contributions, *i.e.*, $M_e \approx M_e^e + M_e^a$. Although the analysis above is very rough, it can provide an intuitive picture for the main dependence of M_e on the system parameters, as will be shown below.

For most orientations under study, it is difficult for the active particles to swim through the narrow gap between the fixed rods, which leads to a strong accumulation of active particles between the rods. The accumulation-induced torque generally tends to rotate the rods to separate them, namely an

anticlockwise (positive) M_e^a on the left rod [see Fig. 1(b)]. Since the magnitude of M_e^a on the fixed rods often is much larger than the entropy-like torque M_e^e due to the significant particle accumulation, the active depletion torque on the left rod is positive for typical orientations (such as $\theta_{le} = 59°$), in contrast to the equilibrium depletion torque, as plotted in Fig. 2(a). Furthermore, the k_θ dependence of M_e results from the fact that a stronger constraint produces a more significant accumulation torque M_e^a (since the active particles can easily pass through the gap between the weakly constrained rods), while M_e^e is hardly influenced by the constraint. To intuitively show the k_θ dependence of the accumulation effect, we separately compute the density maps of active particles for the cases of fixed and free rods, as shown in Fig. 2(c and d), and also give the density difference map between them in Fig. 2(e) to clearly highlight the impact of the constraint on particle accumulation. Although the density map of the active particles for the fixed case is similar in form to that of the free case, the density-difference map indicates that the external constraint can significantly enhance the particle accumulation between two rods. As a result, a stronger constraint causes a larger M_e^a.

For all k_θ, M_e shows a non-monotonic dependence on the rod orientation, with double peaks. Analogous to the non-monotonic behavior of the active depletion force,[49,68] the peaks of M_e occur at the local maximum accumulation of the active particles (M_e^a reaches the local maximum), where the narrowest gap of the two rods is close to the thickness of one- or two-layer particles, *i.e.*, $0.9\sigma_a$ or $2 \times 0.9\sigma_a$, with the prefactor 0.9 accounting for the soft potential. Thus, the orientational angles corresponding to the peaks of M_e are separately around $\theta_{le} = 69.2°$ or $\theta_{le} = 81.0°$, which is consistent with the results in Fig. 2(a).

To further study the accumulation effect, Fig. 2(b) plots the active depletion torque for a small separation between the rod centers $d = 2.5\sigma_a$. In this case, M_e exhibits a similar k_θ dependence to the case of $d = 4\sigma_a$, except for small θ_{le} values, where M_e is insensitive to the change in k_θ and lacks the direction reversal [Fig. 2(b)]. This difference originates from the following fact. For $d = 4.0\sigma_a$, active particles accumulate in the upper concave area between the two rods [gray region in Fig. 1(b)], as shown in Fig. 2(c), producing a positive M_e^a. However, for $d = 2.5\sigma_a$ and small θ_{le} values, the upper concave space between the rods is so narrow that the active particles only reside in the lower concave area between the the two rods [light-green region in Fig. 2(f)], thus generating a negative (clockwise) M_e^a. Independent of k_θ, this negative accumulation torque always tends to push the top ends of the two rods to touch together, inducing a 'self-locking' effect. Thus, the accumulation effect does not depend on the constraint any more as well as M_e^a, such that M_e is not sensitive to k_θ. Note that for the small separation ($d = 2.5\sigma_a$) the equilibrium depletion torque is always negative [inset of Fig. 2(b)].

To check the finite size effect, we also compute M_e for some typical orientations in a larger system (4000 particles). The obtained results (not shown) are almost the same as those of the present system (1000 particles), indicating that the present system size is suitable for achieving correct simulation results.

Active depletion torque for configuration II

We next analyze the active depletion torque M_e for the parallel configuration II. Fig. 3(a) shows M_e as a function of the left rod orientation with $d = 4.0\sigma_a$ for various constraint strength values k ranging from 0 (free) to infinite (fixed). Thanks to the symmetry of the configuration, we only consider M_e on the left rod (identical to that of the right rod). Note that the minimum θ_{le} occurs when the two rods touch together. The non-monotonic orientation dependence of M_e is very similar to the case of configuration I [Fig. 2(a)] due to the same reason. Likewise, the reason for the k_θ dependence of M_e is also the same as that of configuration I, namely, that the external constraint enhances the particle accumulation, as demonstrated by the density difference of active particles between the fixed and free cases in Fig. 3(c). However, there is only a weak constraint dependence of M_e at small θ_{le}, relative to the case of Fig. 2(a). This is since, for small θ_{le} values, such as $\theta_{le} = 24.9°$, the accumulation position of the active particles is close to the rod center [see Fig. 3(d)], *i.e.*, the accumulation torque M_e^a is small because of the short arm of force. In this way, even if the particle accumulation increases with k_θ, the change in M_e is not prominent (the entropy-like torque M_e^e is almost independent of the constraint strength k_θ).

We also compute M_e for a small separation between two rod centers $d = 2.5\sigma_a$, as shown in Fig. 3(b). The M_e value also possesses a significant dependence on the constraint, particularly at small θ_{le}, unlike the situation of $d = 4\sigma_a$ in Fig. 3(a). In Fig. 3(b), the combination of the small separation d and the small θ_{le} shifts the accumulation location of the active particles to the rod ends, *i.e.*, M_e^a with a long arm of force. As a result,

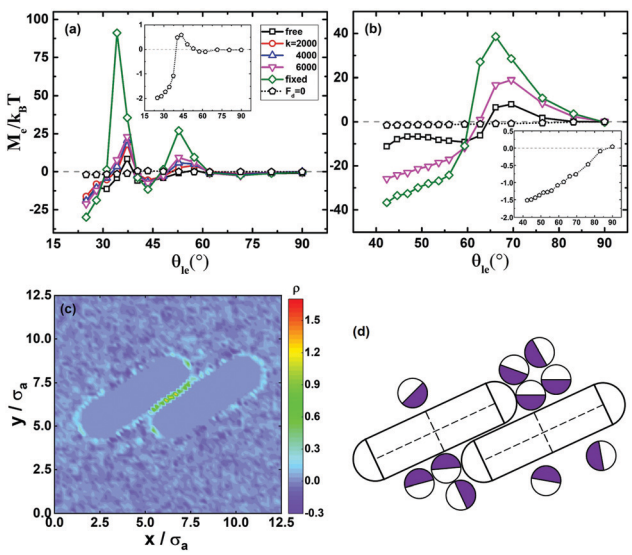

Fig. 3 Configuration II. The reduced active depletion torque as a function of θ_{le} of the left rod with various external constraints for (a) $d = 4.0\sigma_a$ and (b) $d = 2.5\sigma_a$. Insets: The corresponding passive depletion torque. (c) The density difference map of active particles between the fixed and free cases, with $d = 4.0\sigma_a$ and $\theta_{le} = 34.2°$. (d) Active particles accumulate near the centers of the respective rods, with the separation $d = 4.0\sigma_a$ and orientation $\theta_{le} = 24.9°$.

M_e strengthens markedly with the increase of the particle accumulation and hence k_θ. The corresponding passive depletion torques [the insets of Fig. 3(a and b)] can be understood similarly in terms of those for configuration I.

Active depletion torque for configuration III

We now compute the active depletion torque M_e for the asymmetric configuration III. We choose $d = 4.0\sigma_a$ and calculate M_e on the left and right rods as a function of θ_{re} for various k_θ, as plotted in Fig. 4(a) and (b), respectively. Here, the magnitude of M_e on the two rods is slightly different, as the two rods with configuration III are neither symmetric nor equivalent in their configurations [Fig. 1(d)]. Again, the constraint strength k_θ can impact M_e due to the correlation between k_θ and particle accumulation (*i.e.*, M_e^a), which is supported by the density difference of the active particles between the fixed and free cases [Fig. 4(e)]. For comparison, we plot the equilibrium depletion torque in the insets of Fig. 4(a and b). The direction discrepancy between the active and passive depletion torques at their maximum magnitudes arises for the same reason as in Fig. 2(a). In addition, we also compute M_e on the left and right rods for $d = 2.5\sigma_a$, as shown respectively in Fig. 4(c and d), as well as their equilibrium counterparts. The dependence of M_e on the constraints and orientation angle can be similarly understood based on the above analysis.

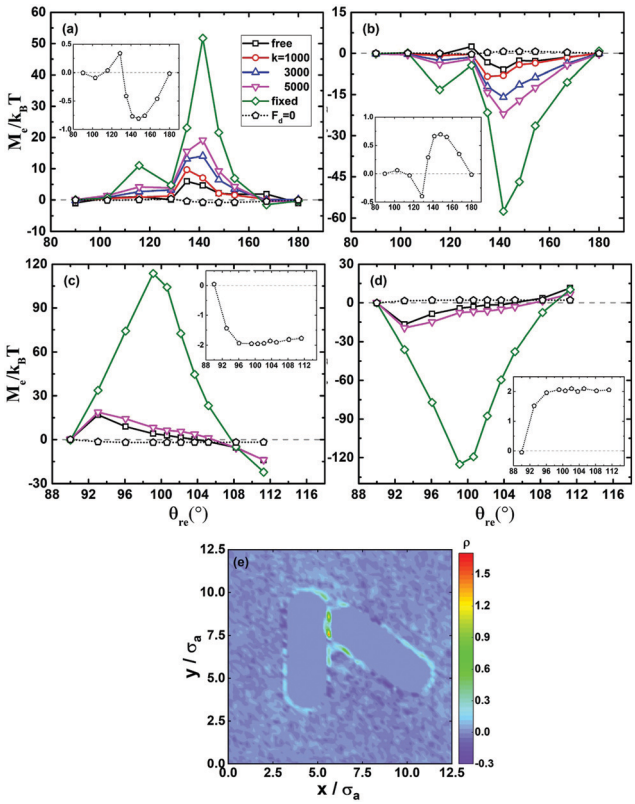

Fig. 4 Configuration III. The reduced active depletion torque on the (a) left and (b) right rods as a function of the orientational angle θ_{re} of the right rod at $d = 4.0\sigma_a$, for various constraint strength values k. The reduced active depletion torque experienced by the (c) left and (d) right rods for $d = 2.5\sigma_a$. Insets: The corresponding passive depletion torques for clarity. (e) The density difference map of active particles between the fixed and free cases, with the separation $d = 4.0\sigma_a$ and orientation $\theta_{re} = 141.4°$.

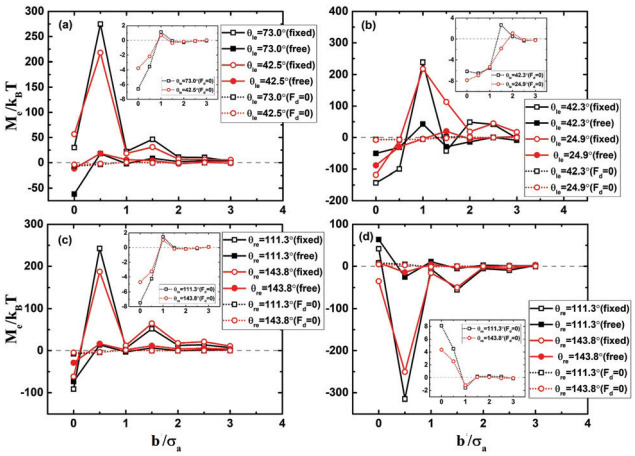

Fig. 5 Reduced active depletion torque as a function of the normalized separation b/σ_a for free and fixed rods, where (a) and (b) refer to the active depletion torques on the left rod for configurations I and II, respectively, and (c) and (d) separately correspond to the torques on the left and right rods for configuration III. The passive depletion torque is plotted in the insets.

Separation dependence of active depletion torque

Finally, in order to investigate the separation dependence of the active depletion torque M_e, we choose two typical rod orientations for each configuration and compute M_e as a function of the minimum surface separation b between the two rods (see Fig. 1) for both free and fixed situations. The M_e data on the left rod for configurations I and II are shown in Fig. 5(a) and (b), respectively, and the M_e values experienced by the left and right rods for configuration III are displayed in Fig. 5(c) and (d), respectively. Moreover, the corresponding equilibrium depletion torques are provided in the insets of Fig. 5. It can be seen that M_e exhibits a non-monotonic behavior as the surface distance b is varied. The reason for this non-monotonicity is the same as for the non-monotonic variation of M_e with the rod orientation in Fig. 2–4, since the change in rod orientation amounts to tuning the surface separation between the two rods, which simultaneously influences the entropy-like torque M_e^e and the accumulation torque M_e^a. Again, the magnitude of M_e on the fixed rod is much higher than that of the free case, except at large surface separations, where M_e basically vanishes. On the other hand, for the same surface separation b, the change in the rod orientation angle can also affect M_e^e and M_e^a, and thus has an impact on the magnitude of M_e, as shown in Fig. 5.

IV Conclusion

Through computer simulations, we systematically study the active depletion torque on two passive rods immersed in an active bath consisting of active Brownian particles. Our results

show that the active depletion torque differs markedly from its passive counterpart in both magnitude and direction. Strikingly, we find that the active depletion torque depends significantly on the external orientational constraint suffered by the rods and may even reverse the direction with the constraint, in stark contrast to the equilibrium depletion torque. The constraint dependence originates mainly from the strong accumulation effect that results from the persistent self-propulsion of the active particles and sensitively hinges on the external constraint. Nevertheless, the active depletion torque hardly changes with the constraint under some special conditions, due to the 'self-locking' effect [Fig. 2(b)] or the vanishing arm of force [Fig. 3(a)]. Our findings provide a deeper insight into understanding biologically-related self-assembly, and could be verified *via* optically trapping non-spherical particles in a bacterial solution, where angular harmonic potentials are created to confine the particles and determine their active effective torques.

Conflicts of interest

There are no conflicts to declare.

Acknowledgements

The authors greatly acknowledge the support of the National Natural Science Foundation of China (No. 11874397, 11674365, and 11974044) and the Strategic Priority Research Program of the Chinese Academy of Sciences (No. XDB33000000).

References

1 A. Rigato, A. Miyagi, S. Scheuring and F. Rico, High-frequency microrheology reveals cytoskeleton dynamics in living cells, *Nat. Phys.*, 2017, **13**(8), 771–775.
2 H. C. Berg, *E. coli in Motion, volume 7 of Biological and Medical Physics. Biomedical Engineering*, Springer New York, New York, NY, 2004, p. 26.
3 R. Sunyer, V. Conte, J. Escribano, A. Elosegui-Artola, A. Labernadie and L. Valon, *et al.*, Collective cell durotaxis emerges from long-range intercellular force transmission, *Science*, 2016, **353**(6304), 1157–1161.
4 H. Li, Xq Shi, M. Huang, X. Chen, M. Xiao and C. Liu, *et al.*, Data-driven quantitative modeling of bacterial active nematics, *Proc. Natl. Acad. Sci. U. S. A.*, 2019, **116**(3), 777–785.
5 S. Liu, S. Shankar, M. C. Marchetti and Y. Wu, Viscoelastic control of spatiotemporal order in bacterial active matter, *Nature*, 2021, **590**(7844), 80–84.
6 J. Palacci, C. Cottin-Bizonne, C. Ybert and L. Bocquet, Sedimentation and effective temperature of active colloidal suspensions, *Phys. Rev. Lett.*, 2010, **105**(8), 088304.
7 J. Palacci, S. Sacanna, A. P. Steinberg, D. J. Pine and P. M. Chaikin, Living crystals of light-activated colloidal surfers, *Science*, 2013, **339**(6122), 936–940.
8 C. Lozano, B. Ten Hagen, H. Löwen and C. Bechinger, Phototaxis of synthetic microswimmers in optical landscapes, *Nat. Commun.*, 2016, **7**(1), 1–10.
9 C. W. Shields IV, K. Han, F. Ma, T. Miloh, G. Yossifon and O. D. Velev, Supercolloidal spinners: Complex active particles for electrically powered and switchable rotation, *Adv. Funct. Mater.*, 2018, **28**(35), 1803465.
10 M. De Corato, X. Arqué, T. Patiño, M. Arroyo, S. Sánchez and I. Pagonabarraga, Self-propulsion of active colloids via ion release: theory and experiments, *Phys. Rev. Lett.*, 2020, **124**(10), 108001.
11 S. Ketzetzi, J. de Graaf and D. J. Kraft, Diffusion-based height analysis reveals robust microswimmer-wall separation, *Phys. Rev. Lett.*, 2020, **125**(23), 238001.
12 F. Schmidt, H. Špová-Jungová, M. Käll, A. Würger and G. Volpe, Non-equilibrium properties of an active nanoparticle in a harmonic potential, *Nat. Commun.*, 2021, **12**(1), 1–9.
13 G. A. Patterson, P. I. Fierens, F. S. Jimka, P. König, A. Garcimartn and I. Zuriguel, *et al.*, Clogging transition of vibration-driven vehicles passing through constrictions, *Phys. Rev. Lett.*, 2017, **119**(24), 248301.
14 O. Dauchot and V. Démery, Dynamics of a self-propelled particle in a harmonic trap, *Phys. Rev. Lett.*, 2019, **122**(6), 068002.
15 M. Paoluzzi, R. Di Leonardo and L. Angelani, Self-sustained density oscillations of swimming bacteria confined in microchambers, *Phys. Rev. Lett.*, 2015, **115**(18), 188303.
16 C. Bechinger, R. Di Leonardo, H. Löwen, C. Reichhardt, G. Volpe and G. Volpe, Active particles in complex and crowded environments, *Rev. Mod. Phys.*, 2016, **88**(4), 045006.
17 U. Khadka, V. Holubec, H. Yang and F. Cichos, Active particles bound by information flows, *Nat. Commun.*, 2018, **9**(1), 1–9.
18 M. Fernández-Medina, M. A. Ramos-Docampo, O. Hovorka, V. Salgueiriño and B. Städler, Recent advances in nano-and micromotors, *Adv. Funct. Mater.*, 2020, **30**(12), 1908283.
19 M. E. Cates and J. Tailleur, When are active Brownian particles and run-and-tumble particles equivalent? Consequences for motility-induced phase separation, *EPL*, 2013, **101**(2), 20010.
20 M. E. Cates and J. Tailleur, Motility-induced phase separation, *Annu. Rev. Condens. Matter Phys.*, 2015, **6**(1), 219–244.
21 P. Digregorio, D. Levis, A. Suma, L. F. Cugliandolo, G. Gonnella and I. Pagonabarraga, Full phase diagram of active Brownian disks: From melting to motility-induced phase separation, *Phys. Rev. Lett.*, 2018, **121**(9), 098003.
22 C. B. Caporusso, P. Digregorio, D. Levis, L. F. Cugliandolo and G. Gonnella, Motility-induced microphase and macrophase separation in a two-dimensional active Brownian particle system, *Phys. Rev. Lett.*, 2020, **125**(17), 178004.
23 L. Caprini, U. M. B. Marconi and A. Puglisi, Spontaneous velocity alignment in motility-induced phase separation, *Phys. Rev. Lett.*, 2020, **124**(7), 078001.
24 A. Aubret, M. Youssef, S. Sacanna and J. Palacci, Targeted assembly and synchronization of self-spinning microgears, *Nat. Phys.*, 2018, **14**(11), 1114–1118.
25 H. Massana-Cid, F. Meng, D. Matsunaga, R. Golestanian and P. Tierno, Tunable self-healing of magnetically propelling colloidal carpets, *Nat. Commun.*, 2019, **10**(1), 1–8.

26 J. X. Chen, R. Yuan, R. Cui and L. Qiao, The dynamics and self-assembly of chemically self-propelled sphere dimers, *Nanoscale*, 2021, **13**(2), 1055–1060.
27 P. Arora, A. Sood and R. Ganapathy, Emergent stereo-selective interactions and self-recognition in polar chiral active ellipsoids, *Sci. Adv.*, 2021, **7**(9), eabd0331.
28 T. Vicsek and A. Zafeiris, Collective motion, *Phys. Rep.*, 2012, **517**(3–4), 71–140.
29 A. Bricard, J. B. Caussin, N. Desreumaux, O. Dauchot and D. Bartolo, Emergence of macroscopic directed motion in populations of motile colloids, *Nature*, 2013, **503**(7474), 95–98.
30 P. Liu, H. Zhu, Y. Zeng, G. Du, L. Ning and D. Wang, *et al.*, Oscillating collective motion of active rotors in confinement, *Proc. Natl. Acad. Sci. U. S. A.*, 2020, **117**(22), 11901–11907.
31 R. Alert, J. Casademunt and J. F. Joanny, Active turbulence, *Annu. Rev. Condens. Matter Phys.*, 2021, **13**, 143–170.
32 A. P. Solon, Y. Fily, A. Baskaran, M. E. Cates, Y. Kafri and M. Kardar, *et al.*, Pressure is not a state function for generic active fluids, *Nat. Phys.*, 2015, **11**(8), 673–678.
33 S. Ye, P. Liu, F. Ye, K. Chen and M. Yang, Active noise experienced by a passive particle trapped in an active bath, *Soft Matter*, 2020, **16**(19), 4655–4660.
34 L. Angelani, R. Di Leonardo and G. Ruocco, Self-starting micromotors in a bacterial bath, *Phys. Rev. Lett.*, 2009, **102**(4), 048104.
35 R. Di Leonardo, L. Angelani, D. DellArciprete, G. Ruocco, V. Iebba and S. Schippa, *et al.*, Bacterial ratchet motors, *Proc. Natl. Acad. Sci. U. S. A.*, 2010, **107**(21), 9541–9545.
36 A. Sokolov, M. M. Apodaca, B. A. Grzybowski and I. S. Aranson, Swimming bacteria power microscopic gears, *Proc. Natl. Acad. Sci. U. S. A.*, 2010, **107**(3), 969–974.
37 T. Speck, Collective forces in scalar active matter, *Soft Matter*, 2020, **16**(11), 2652–2663.
38 P. Liu, S. Ye, F. Ye, K. Chen and M. Yang, Constraint dependence of active depletion forces on passive particles, *Phys. Rev. Lett.*, 2020, **124**(15), 158001.
39 S. Asakura and F. Oosawa, On interaction between two bodies immersed in a solution of macromolecules, *J. Chem. Phys.*, 1954, **22**(7), 1255–1256.
40 J. Stenhammar, R. Wittkowski, D. Marenduzzo and M. E. Cates, Activity-induced phase separation and self-assembly in mixtures of active and passive particles, *Phys. Rev. Lett.*, 2015, **114**(1), 018301.
41 P. Dolai, A. Simha and S. Mishra, Phase separation in binary mixtures of active and passive particles, *Soft Matter*, 2018, **14**(29), 6137–6145.
42 H. Massana-Cid, J. Codina, I. Pagonabarraga and P. Tierno, Active apolar doping determines routes to colloidal clusters and gels, *Proc. Natl. Acad. Sci. U. S. A.*, 2018, **115**(42), 10618–10623.
43 L. Angelani, Spontaneous assembly of colloidal vesicles driven by active swimmers, *J. Phys.: Condens. Matter*, 2019, **31**(7), 075101.
44 S. Ramananarivo, E. Ducrot and J. Palacci, Activity-controlled annealing of colloidal monolayers, *Nat. Commun.*, 2019, **10**(1), 1–8.
45 M. Abercrombie, C. J. Hickman and M. L. Johnson, *A dictionary of biology*, Routledge, 2017.
46 R. Zhang, S. A. Redford, P. V. Ruijgrok, N. Kumar, A. Mozaffari and S. Zemsky, *et al.*, Spatiotemporal control of liquid crystal structure and dynamics through activity patterning, *Nat. Mater.*, 2021, **20**, 875–882.
47 A. Sciortino and A. R. Bausch, Pattern formation and polarity sorting of driven actin filaments on lipid membranes, *Proc. Natl. Acad. Sci. U. S. A.*, 2021, **118**(6), e2017047118.
48 L. Angelani, C. Maggi, M. Bernardini, A. Rizzo and R. Di Leonardo, Effective interactions between colloidal particles suspended in a bath of swimming cells, *Phys. Rev. Lett.*, 2011, **107**(13), 138302.
49 R. Ni, M. A. C. Stuart and P. G. Bolhuis, Tunable long range forces mediated by self-propelled colloidal hard spheres, *Phys. Rev. Lett.*, 2015, **114**(1), 018302.
50 C. M. Kjeldbjerg and J. F. Brady, Theory for the Casimir effect and the partitioning of active matter, *Soft Matter*, 2021, **17**(3), 523–530.
51 F. Feng, T. Lei and N. Zhao, Tunable depletion force in active and crowded environments, *Phys. Rev. E*, 2021, **103**(2), 022604.
52 Y. Baek, A. P. Solon, X. Xu, N. Nikola and Y. Kafri, Generic long-range interactions between passive bodies in an active fluid, *Phys. Rev. Lett.*, 2018, **120**(5), 058002.
53 O. Granek, Y. Baek, Y. Kafri and A. P. Solon, Bodies in an interacting active fluid: Far-field influence of a single body and interaction between two bodies, *J. Stat. Mech.: Theor. Exp.*, 2020, **6**, 063211.
54 R. Roth, R. van Roij, D. Andrienko, K. Mecke and S. Dietrich, Entropic torque, *Phys. Rev. Lett.*, 2002, **89**(8), 088301.
55 W. Li and H. Ma, Depletion force and torque on an ellipsoid, *J. Chem. Phys.*, 2003, **119**(1), 585–589.
56 W. Li and H. Ma, Depletion interactions between two spherocylinders, *Eur. Phys. J. E: Soft Matter Biol. Phys.*, 2005, **16**(2), 225–231.
57 H. Miao, Y. Li and H. Ma, Depletion interaction between two ellipsoids, *J. Chem. Phys.*, 2014, **140**(15), 154904.
58 D. Andrienko, M. P. Allen, G. Skacej and S. Žumer, Defect structures and torque on an elongated colloidal particle immersed in a liquid crystal host, *Phys. Rev. E: Stat., Nonlinear, Soft Matter Phys.*, 2002, **65**(4), 041702.
59 P. M. König, R. Roth and S. Dietrich, Depletion forces between nonspherical objects, *Phys. Rev. E: Stat., Nonlinear, Soft Matter Phys.*, 2006, **74**(4), 041404.
60 P. M. König, R. Roth and S. Dietrich, Lock and key model system, *EPL*, 2009, **84**(6), 68006.
61 G. van Anders, D. Klotsa, N. K. Ahmed, M. Engel and S. C. Glotzer, Understanding shape entropy through local dense packing, *Proc. Natl. Acad. Sci. U. S. A.*, 2014, **111**(45), E4812–E4821.
62 G. van Anders, N. K. Ahmed, R. Smith, M. Engel and S. C. Glotzer, Entropically patchy particles: Engineering valence through shape entropy, *ACS Nano*, 2014, **8**(1), 931–940.
63 S. Sacanna, W. T. Irvine, P. M. Chaikin and D. J. Pine, Lock and key colloids, *Nature*, 2010, **464**(7288), 575–578.

64 H. Löwen, Brownian dynamics of hard spherocylinders, *Phys. Rev. E: Stat., Nonlinear, Soft Matter Phys*, 1994, **50**(2), 1232.
65 S. C. Takatori and J. F. Brady, A theory for the phase behavior of mixtures of active particles, *Soft Matter*, 2015, **11**(40), 7920–7931.
66 S. C. Takatori, R. De Dier, J. Vermant and J. F. Brady, Acoustic trapping of active matter, *Nat. Commun.*, 2016, **7**(1), 1–7.
67 T. Jamali and A. Naji, Active fluids at circular boundaries: swim pressure and anomalous droplet ripening, *Soft Matter*, 2018, **14**(23), 4820–4834.
68 M. Zaeifi Yamchi and A. Naji, Effective interactions between inclusions in an active bath, *J. Chem. Phys.*, 2017, **147**(19), 194901.

